EASR

Engineering and Applied Science Research

https://www.tci-thaijo.org/index.php/easr/index

Published by the Faculty of Engineering, Khon Kaen University, Thailand

Decolorization of indigo carmine dye using silver nanoparticles synthesized via green method mediated by *Leucaena leucocephala*: A response surface methodology

Pharini Chaison[1)], Wimonrat Tongpoothorn[2)], Kitiyaporn Wittayanarakul[3)] and Manop Sriuttha*[3)]

[1)]Program in Applied Bioresource Science, Faculty of Interdisciplinary Studies, Khon Kaen University, Nong Khai Campus, Nong Khai 43000, Thailand
[2)]Department of Chemistry, Faculty of Engineering, Rajamangala University of Technology Isan, Khon Kaen Campus, Khon Kaen 40000, Thailand
[3)]Program in Science Technology and Business Enterprise, Faculty of Interdisciplinary Studies, Khon Kaen University, Nong Khai Campus, Nong Khai 43000, Thailand

Received 5 May 2024
Revised 27 August 2024
Accepted 4 September 2024

Abstract

This study aims to synthesize and characterize silver nanoparticles (AgNPs) from *Leucaena leucocephala* leaf extract and evaluate their effectiveness in photo-catalytically degrading indigo carmine (IC) dye in an aqueous solution. The synthesized AgNPs were characterized using UV-visible spectrophotometry (UV-Vis), diffuse reflectance spectroscopy (DRS), Fourier transform infrared spectroscopy (FTIR), energy dispersive X-ray spectroscopy (EDX), transmission electron microscopy (TEM), and X-ray diffraction (XRD) techniques. Response surface methodology (RSM) based on central composite design (CCD) was employed to optimize the conditions for the photocatalytic degradation of IC dye under solar light. The results show that 97.52% of the maximum photodegradation of IC dye was achieved using a dye concentration, catalyst volume, and reaction time of 19.7 mgL^{-1}, 4.47 mL, and 97 min, respectively. RSM results revealed optimal conditions for IC dye degradation under solar irradiation. Moreover, the kinetics study of IC dye showed a good correlation with the pseudo-first order kinetic model.

Keywords: Silver nanoparticles, *Leucaena leucocephala*, Photocatalytic degradation, Indigo carmine, Central composite design, Response surface methodology

1. Introduction

Numerous pollutants have negative effects on ecosystems, as well as on the health of animals, plants, and people. Several industries generate liquid or gaseous effluents that negatively impact human health and safety [1]. Industrial effluents are a primary contributor to environmental pollution. Many industries that produce food, textiles, medicines, and cosmetics, extensively employ dyes to color their products to suit customer preferences [2]. However, depending on their application and composition, some effluents can be toxic to aquatic life [3]. Effluents from the dyeing industry contain high levels of suspended organic material [4]. Among several dye types, indigo carmine (IC) dye is the oldest and most widely used in the textile, food, and cosmetics industries. In high concentrations, IC dye effluents are poisonous and cause a variety of health issues, such as skin and eye irritation [5]. One of the most important industrial management responsibilities is to remove this dye from effluents before releasing them into the ecosystem. To remove organic contaminants such as IC dye from wastewater, a wide range of chemical, physical, and biological methods have been investigated [6]. Some removal methods using processes that coagulate organic material produce much sludge. However, most of these dyes are highly resistant to biodegradation and photodegradation. Therefore, these primary pollutants may react to form even more toxic secondary pollutants [7]. Adsorption, ozonolysis, chemical processes, biodegradation, and photocatalytic degradation have been extensively utilized to eliminate toxic dyes from effluents. Photocatalytic degradation is a useful method for removing dyes from wastewater. This technique indicates the potential impact on a wide spectrum of pollutant mineralization [8]. Recently, production of green nanoparticles has received attention for their use in degrading environmental contaminants [9]. Photocatalytic degradation utilizing nanoparticles (NPs) offers numerous advantages over other techniques. These advantages include high efficiency, selectivity, environmental compatibility, adaptability, and cost-effectiveness [10]. Recently, nanoparticles were used as catalysts to degrade dyes in several photocatalytic processes, as depicted in Table 1.

*Corresponding author.
Email address: manosr@kku.ac.th
doi: 10.14456/easr.2024.60

Table 1 Nanoparticles as catalysts for photocatalytic degradation of dyes

Catalyst	Dye pollutant	Reaction conditions	Performance	Light source	Ref.
AgNPs	MO	Pollutant: 10 mg L^{-1} Catalyst: 0.2 g	95.47%, 7 min	Solar light	[9]
Ag-doped ZnO NPs	MB	Pollutant: 10 mg L^{-1} Catalyst: 15 mg pH: Neutral	98%, 120 min	Solar light	[11]
AgNPs	CR	Pollutant: 10 mg L^{-1} Catalyst: 1 g pH: 8	<95%, 150 min	UV light	[12]
AgNPs	RhB	Pollutant: 20 μM Catalyst: 0.09 g	95%, 75 min	Solar light	[13]
ZnO NPs	MB	Pollutant: 20 μM Catalyst: 0.09 g	98.50%, 60 min	Solar light	[14]

Metal nanoparticles such as gold, platinum, and silver play significant roles in various industries including electronics, biological applications, environmental remediation, medicine, and catalysis. Silver nanoparticles (AgNPs) have been widely used in numerous applications due to their exceptional catalytic, antibacterial, and anti-inflammatory properties [15]. Green NP synthesis has many advantages over physical and chemical techniques including being non-toxic, more stable, economical, and environmentally beneficial [16]. Eco-friendly procedures for synthesizing NPs involve utilizing plant extracts or other natural resources as precursors employing no hazardous chemicals. Using plant extracts for NP synthesis is a safe method due to their non-toxic nature [17]. In previous studies, AgNPs can be synthesized via green methods using various plant extracts, which exhibit differences in size and shape, as shown in Table 2.

Table 2 Nanomaterials prepared from several plant extracts

Plant	Part	Condition	Characteristics	Ref.
Salvia (*Salvia tebesana*)	Leaves	Extract: 1 gL^{-1} $AgNO_3$: 10 mM pH: 12 Method: stirring Temp: 55 °C Time: 30 min	SPR peak: 415 nm Shape: spherical Size: 10-15 nm	[18]
Alfalfa (*Medicago sativa*)	Seeds	Extract: 10 mL $AgNO_3$: 10 mM pH: 12 Time: 60 min Temp: 85 °C	SPR peak: 419 Shape: spherical/elliptical Size: 13-15 nm	[19]
Moringa (*Moringa oleifera*)	Leaves	Extract: 20 mL $AgNO_3$: 3 mM Method: stirring Time: 24 h Temp: Ambient	SPR peak: 477 nm Shape: spherical Size: 25.235 ± 0.694 nm	[20]
Heartleaf hempvine (*Mikania cordata*)	Leaves	Extract: 40 mL $AgNO_3$: 1 M Method: shaking Time: 70 min Temp: 80 °C	SPR peak: 451 nm Shape: spherical Size: 26.8 - 46.0 nm	[21]
Clove (*Syzygium aromaticum*)	Flower buds	Extract: 10 mL $AgNO_3$: 1 mM pH: 10 Method: stirring Time: 25 min Temp: 40 °C	SPR peak: 410 nm Shape: spherical Size: 12.34 ± 1.90 nm	[22]

Leucaena leucocephala is a medium-sized, rapidly growing tree in the *Fabaceae* family. Its extracts exhibit remarkable medicinal properties, but it is also among the 100 most invasive species in the world. The species is reported to be an aggressive colonizer, forming dense monospecies stands that threaten native plant communities [23, 24]. Therefore, it is necessary to reduce the population density of this species. Scientific evaluation has shown that *Leucaena leucocephala* contains phytochemical substances such as tannins, coumarins, saponins, flavonoids, steroids, cardiac glycosides, amino acids, carbohydrates, and phenols. Furthermore, the analysis of phytochemical compounds in *Leucaena leucocephala* leaf extract using HPLC techniques found that the leaves contain a substantial amount of rosmarinic acid, resveratrol, and quercetin, which have potential antioxidant activities [25]. Additionally, *Leucaena leucocephala* leaf extracts serve as both reducing and stabilizing agents, as well as a capping agent for the green synthesis of AgNPs. Biogenic AgNPs demonstrate exceptional photocatalytic properties in the treatment of effluents containing organic dyes, indicating their potential as effective agents for environmental remediation [26].

Utilization of green synthesized NPs provides photocatalysts that can effectively degrade toxic dyes. Therefore, for this specific goal, evaluation of environmentally friendly synthesis and characterization of NPs are essential for developing photocatalytic degradation methods [10]. Several parameters were studied for determination of the optimal conditions for IC degradation utilizing AgNPs, including dye concentration, catalyst volume, and reaction time under solar irradiation. Nonetheless, basic experimental

analysis may limit the simultaneous investigation of more than two variable parameters. Response surface methodology (RSM), a statistical technique widely employed in experimental design, has proven effective in optimizing complicated systems. It reduces development costs and time, improves production response to nominally meet goal requirements, and decreases process instability [27].

The objectives of this research are to synthesize AgNPs using *Leucaena leucocephala* extract and to evaluate their photocatalytic properties for IC dye degradation. The characteristics of AgNPs were investigated using UV-visible spectrophotometry (UV-Vis), diffuse reflectance spectroscopy (DRS), Fourier transform infrared spectroscopy (FTIR), energy dispersive X-ray spectroscopy (EDX), transmission electron microscopy (TEM), and X-ray diffraction (XRD) techniques. RSM was used to optimize the parameters of the photocatalytic process. Three parameters were evaluated including the concentrations of IC dye, volume of catalyst, and reaction time. Additionally, a kinetics study was done to investigate the rate of dye degradation.

2. Materials and methods

2.1 Materials and chemicals

Silver nitrate ($AgNO_3$) was obtained from Fisher Chemical, UK. Indigo carmine ($C_{16}H_8N_2Na_2O_8S_2$) was purchased from Loba Chemie, India. The leaves of *Leucaena leucocephala* were gathered from the grounds of Khon Kaen University, Nong Khai Campus, Nong Khai, Thailand. Deionized water (DI) was used to prepare all solutions.

2.2 Preparation of Leucaena leucocephala leaf extract

To remove contaminants, the leaves of *Leucaena leucocephala* were washed several times with tap water. The collected leaves were air-dried at ambient temperature in a shaded area. Next, a fine powder was obtained from dried leaves using a blender and passing the material through a sieve stack on a shaker, using material passing a Number 10 sieve (<2 mm particle size). The resulting powder was then subsequently stored in a plastic container at ambient temperature. For preparation of leaf extract solutions, 5 g of the powder and 200 mL of DI water were combined and heated in a microwave oven at 300 W for 2 min. It was subsequently allowed to cool to ambient temperature and filtered through Whatman No. 1 filter paper. The filtrate solution was stored at 4 °C for further use.

2.3 Green synthesis of AgNPs

The extract from *Leucaena leucocephala* leaves was used as a reducing agent in an eco-friendly method to synthesize AgNPs. AgNP synthesis was done under optimal conditions using RSM (data not shown). Under these optimal conditions, the leaf extract (400 µL) was combined with 2.75 mM $AgNO_3$ (10 mL). The mixture was subsequently heated in a microwave oven at 600 W for 2 min. The mixed solution was left to stand at room temperature for 1 h [28]. Next, 25 mL of the mixed solution was transferred into a volumetric flask. UV-Vis spectrometry was used to monitor the transformation of AgNPs in the wavelength range of 300-800 nm [29]. The color of the mixture changed noticeably from light yellow to reddish-brown.

2.4 Characterization of AgNPs

The absorbance data were recorded using a UV-Visible spectrophotometer (UV-1900i, Shimadzu, Japan). DRS was used to determine the band energy of AgNPs using Tauc's relation [30]. The functional groups of AgNPs were analyzed using Fourier transform infrared spectroscopy (TENSOR 27, Bruker, USA). The chemical composition, particle size, and surface morphology of AgNPs were investigated by employing TEM and EDX techniques (TECNAI G2 20, FEI, USA). Crystallography of AgNPs was examined using an X-ray diffractometer (EMPYREAN, Bruker, USA).

2.5 Photocatalytic decolorization of IC dye

To determine the photocatalytic efficiency of the synthesized AgNPs, degradation of IC dye under solar light was monitored using spectroscopic absorbance. RSM values served to predict optimal performance. Three parameters, including dye concentration (2-10 mgL^{-1}), catalyst volume (0.5-5.5 mL), and reaction time (20-120 min), were optimized to evaluate the degradation of IC dye. Various concentrations of IC (20 mL) were mixed with different volumes of AgNPs catalyst. Mixture solutions were adjusted with DI water to a final volume of 30 mL [31]. The studies were carried out at a pH of 5.6, which represents the natural solution for the dissolution of the desired molecules in DI water [32]. The mixture solutions were shaken for 30 min in the dark at 150 rpm to achieve adsorption/desorption equilibrium and enhance the dispersion of the AgNPs catalyst in the mixture solution [33]. The reactions were conducted at different time intervals in daylight from 11:00 a.m. to 1:00 p.m. [34]. An aliquot (6 mL) of each run was taken and centrifuged, and then the absorbance was measured to determine the degradation percentage [35]. IC concentration was determined using UV-Vis absorbance at 610 nm. The degradation performance of the catalysts was evaluated according to Eq. (1).

$$dye\ degradation\ (\%) = \frac{C_0 - C}{C_0} \times 100 \quad (1)$$

where C_0 and C are respectively the initial and final concentrations of IC dye over the course of its photocatalytic degradation [36].

2.6 Kinetics study

Kinetics studies were performed using the optimal conditions of AgNP catalyst volumes and dye concentrations at different times. The samples were examined at appropriate intervals until they reached an equilibrium state [37]. An adsorption/desorption equilibrium

was achieved by agitating the mixed solutions for 30 min at 150 rpm in the dark. The reactions were conducted at different time intervals under daylight conditions from 11:00 a.m. to 1:00 p.m. [34]. The solutions were then centrifuged for 5 min at 9,000 rpm [35]. Change in dye concentration was determined by measuring sample absorbance at 610 nm using a UV-Vis technique. Kinetics data of dye degradation were evaluated using pseudo-first order (Eq. 2) and pseudo-second order (Eq. 3) equations [38, 39].

$$\ln(C/C_0) = -k_1 \mathrm{t} \tag{2}$$

$$\frac{t}{C} = \frac{t}{C_0} - \frac{1}{k_2 C_0^2} \tag{3}$$

where C_0, C, t, k_1, k_2 are the initial concentration, the concentration at a given time, the time of reaction, the rate constant of pseudo-first order (min^{-1}), and the rate constant of pseudo-second order (mg^{-1} L min^{-1}) equations, respectively.

2.7 Experimental design and data analysis

Photocatalytic degradation of IC dye was optimized using response surface methodology (RSM) based on CCD. This method is suitable for modeling quadratic surfaces and helps to reduce the number of experiments needed to optimize the parameters and analyze their interactions. RSM was employed to assess the photocatalytic process by considering reaction time, catalyst volume, and dye concentration. There was a total of 20 trials conducted using a 2^4 full factorial CCD. The designations for the equally spaced x_i values are -α, -1, 0, +1, +α. The independent variables, levels, and experimental ranges are shown in Table 3.

Table 3 Experimental design of independent variables and coded levels for the photocatalytic degradation of IC dye

Independent variable	Coded levels				
	-α	**-1**	**0**	**+1**	**+α**
A: Dye concentration (mgL^{-1})	10.0	18.1	30.0	41.9	50.0
B: Catalyst volume (mL)	0.50	1.51	3.00	4.49	5.50
C: Reaction time (min)	20	40	70	100	120

Regression coefficients were obtained after experimental data were evaluated using Design-Expert 13 (trial version) and fitted to a second-order polynomial model. This program was employed to create two-dimensional contour plots, three-dimensional curves, and residual plots of the response surfaces. In conducting the response (Y) surface analysis, the following generalized second-order polynomial model was employed:

$$Y = \beta_0 + \sum_{i=1}^{k} \beta_i X_i + \sum_{i=1}^{k} \beta_{ii} X_i^2 + \sum_{i=1}^{k} \sum_{j=1}^{k} \beta_{ij} X_i X_j + e_0 \tag{4}$$

where Y is the response (%degradation); β_0 is a constant coefficient (free term or intercept constant); β_i is the coefficients of the linear effects (or first-order effect) of parameter X_i; β_{ii} is the quadratic coefficients (second-order regression coefficients); β_{ij} values are the interactions effects between the independent variables X_i and X_j; X_i and X_j are independent variables which are considered to influence the response; k =3 is the number of independent parameters; i and j are the index numbers of patterns; e_0 represents model error (giving the uncertainties between the predicted and the actual values of the parameters) [32]. The polynomial model was subjected to an analysis of variance (ANOVA) at a 95% confidence level to determine its statistical significance. Additionally, the quality of the model fit was assessed using a residual plot. The coefficient of determination (R^2) expresses how well the polynomial modeled the data.

3. Results and discussion

3.1 Characterization of AgNPs

3.1.1 UV-Vis analysis

Aqueous solutions of green AgNPs synthesized using *Leucaena leucocephala* leaf extract were compared to the control solutions ($AgNO_3$ and *Leucaena leucocephala* leaf extract), as the color changed from light-yellow to reddish-brown. Under identical conditions, the control solutions showed no absorption band (Figure 1(a)). The AgNP absorption peak observed at 417 nm is caused by surface plasmon resonance (SPR), which occurs when free electrons in the metal are excited during the synthesis of AgNPs. This suggests that the optical properties of the $AgNO_3$ solutions were changed due to the reduction of Ag^+ to Ag^0 or AgNPs upon exposure to the bioactive constituents of the plant extract [40].

3.1.2 DRS analysis

DRS analysis was performed to investigate the light absorption properties of green synthesized AgNPs [8]. Figure 1(b) shows the DRS analysis of AgNPs synthesized using *Leucaena leucocephala* extract. The synthesized AgNPs have an absorption edge around 417 nm, corresponding to a band gap of 2.34 eV. The DRS investigation showed that the green synthesized AgNPs had a strong capability to absorb light in the visible range. Several strategies have been investigated to sensitize AgNPs to visible light for applications in photocatalytic degradation [41]. The low band gap facilitated efficient electron-hole pair generation under visible light irradiation, enhancing the photocatalytic performance of the AgNPs [41, 42]. The band gap energy of the green synthesized AgNPs is like that of AgNPs synthesized using plant extracts in a previous study [31].

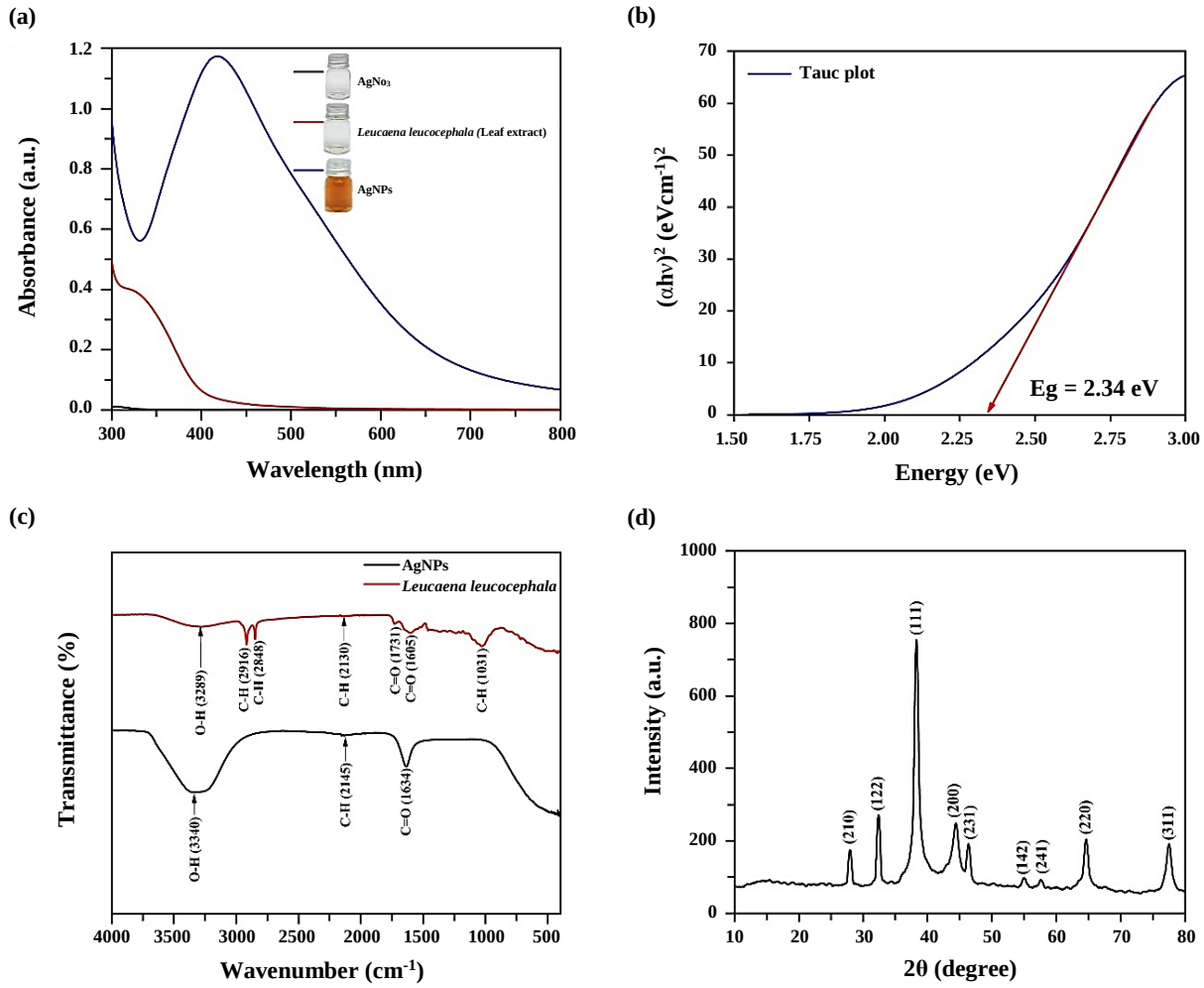

Figure 1 UV-Vis absorption spectra of $AgNO_3$, leaf extract of *Leucaena leucocephala*, and AgNPs (a), DRS of AgNPs showing E_g = 2.34 eV (b), FTIR spectra of AgNPs and leaf powder of *Leucaena leucocephala* (c), and XRD of AgNPs (d)

3.1.3 FTIR analysis

FTIR analysis of *Leucaena leucocephala* leaf extract revealed the presence of various functional groups including hydroxyl, carbonyl, amine, and alkyl halides, which can interact with silver ions and facilitate their reduction to AgNPs [23, 43]. Figure 1(c) shows the FTIR spectrum of the leaf extract of *Leucaena leucocephala*, displaying seven distinct bands at different wavenumbers, 3289, 2916, 2848, 2130, 1731, 1605, and 1013 cm^{-1}. These bands represent three different functional groups, O-H stretching, C-H stretching, and C=O stretching, indicating the involvement of biomolecules such as alcohols and phenols in AgNP synthesis [23, 40]. The FTIR spectra showed a shift in peak positions after AgNP formation, suggesting that the phytochemicals bind to nanoparticle surfaces and act as capping and stabilizing agents. Comparing the FTIR spectra of *Leucaena leucocephala* leaf extract and the synthesized AgNPs revealed distinct differences, confirming the activity of phytochemicals in the bioreduction process [43, 44]. FTIR peaks became more intense after AgNP formation, indicating an increased concentration of functional groups during synthesis [23]. The FTIR analysis confirmed the presence of biomolecules such as polyphenols on AgNP surfaces, which contributed to their stability and prevented aggregation [23, 44]. Capping of AgNPs by the phytochemicals also influenced their size, shape, and dispersity, as is evident from the FTIR spectra [43, 44].

3.1.4 XRD analysis

XRD was employed to investigate the crystal size and structure of nanoparticles. Figure 1(d) shows the XRD patterns of green synthesized AgNPs, in which diffraction peaks located at 2θ angles of 27.98°, 32.35°, 38.20°,44.29°, 46.35°, 55.00°, 57.52°, 64.72°, and 77.49° can be attributed to the (210), (122), (111), (200), (231), (142), (241), (220), and (311) planes of pure silver, based on the face-centered cubic (FCC) structure (JCPDS standard data, Card No. 04-0783). The XRD data reveal that the AgNPs generated by the extract have a crystalline nature [45].

3.1.5 TEM analysis

The morphology and size of the green synthesized AgNPs were evaluated using TEM. The TEM imagery of AgNPs at various magnifications are presented in Figures 2(a) and 2(b), showing spherical shapes. Identification of single crystal AgNPs is supported by the lattice fringes depicted in Figure 2(b). Additionally, the interplanar spacing (d) of AgNPs, is d = 0.232 nm. This value is consistent with the reported value of the (111) plane spacing for the FCC structure of silver [46]. Furthermore, Figure 2 (c) displays a histogram

of the particle diameter size distribution of the green synthesized AgNPs. This histogram was created using Image-J software. The average particle size and their distribution was 7.29 ± 0.05 nm [15].

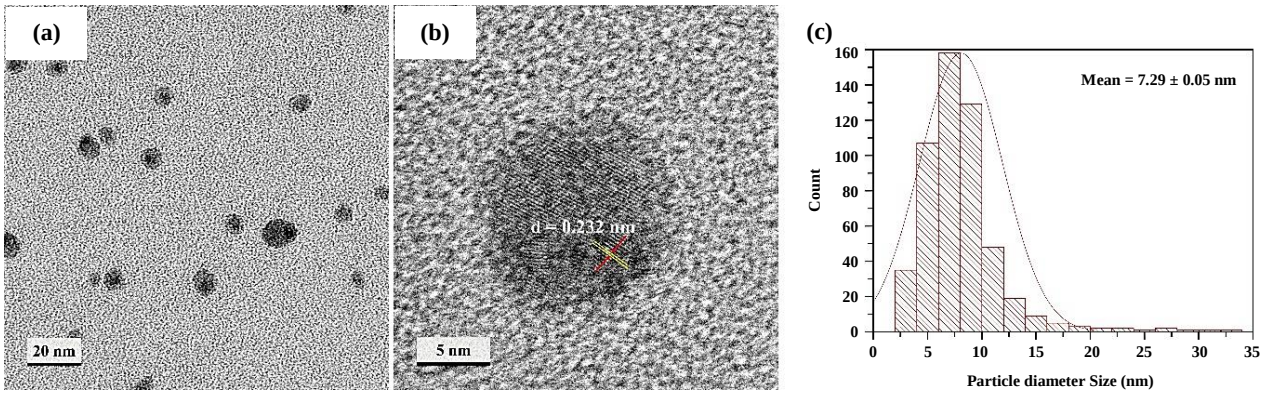

Figure 2 TEM imagery was analyzed at 20 nm (a), and 5 nm (b); particle diameter distribution histogram of AgNPs (c)

3.1.6 EDX analysis

The elemental composition of green-synthesized AgNPs was determined using EDX analysis, and the results are shown in Figure 3. Green synthesized AgNPs exhibited dominant peaks that indicate the presence of elemental silver (Ag), along with additional minor peaks corresponding to other elements. The presence of characteristic peaks of carbon (C), and chlorine (Cl) can be explained by the presence of carbohydrates and proteins in the cellular structure. These organic compounds may have acted as capping agents or stabilizers during AgNP synthesis. The carbon peak showed that the leaf extract of *Leucaena leucocephala* is the source of phytochemicals that stabilize AgNPs. Furthermore, peaks of other elements, such as Cu, were also discovered, since the TEM grids were made of Cu [47, 48].

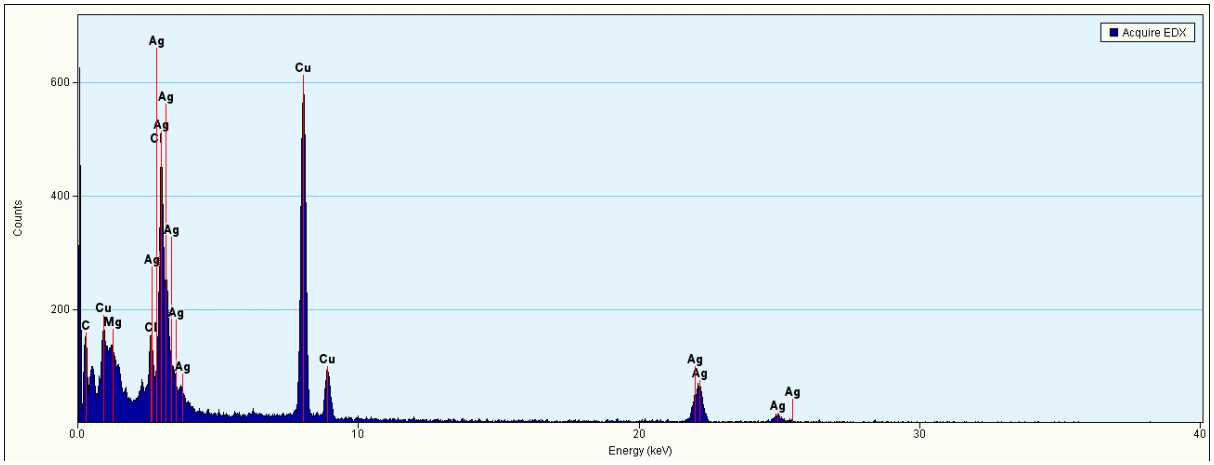

Figure 3 The EDX spectrum of AgNPs

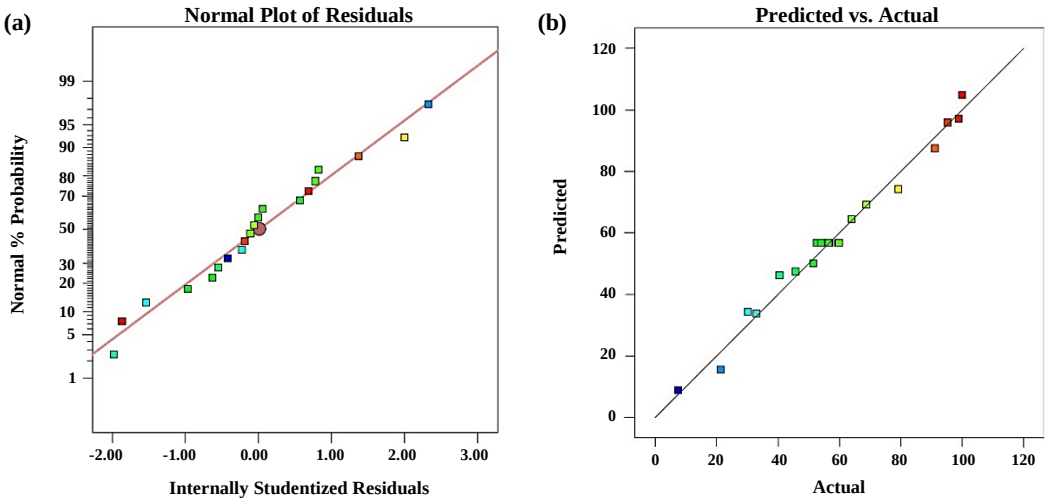

Figure 4 Normal plot of residuals vs. internally studentized residuals (a) and predicted vs. actual data (b) for degradation efficiency of IC dye

3.2 Photocatalytic decolorization of IC dye

3.2.1 Optimization of photocatalytic degradation of IC dye

The residuals exhibited a normal distribution due to their close alignment with a straight line, as depicted in Figure 4(a) [49]. Figure 4(b) shows that the actual values of IC degradation from the experiments closely align with the predicted values, forming a linear trend line. It is clear that the model was accurate based on the relationship between experimental data on the photocatalytic degradation of IC and predicted values. The experimental data are symmetrically arranged within the confidence level, as illustrated by the graphs in Figure 4. This demonstrates that the quadratic model is suitable [50].

Statistically designed experiments were conducted to assess the effect of various parameters. Table 4 shows the experimental design matrix, with predicted and observed values of IC dye degradation efficiencies.

Table 4 Variables of CCD along with predicted and actual values for the photocatalytic degradation of IC dye

Run	Variables in coded levels			Degradation (%)	
	A: Dye concentration (mgL^{-1})	B: Catalyst volume (mL)	C: Reaction time (min)	Predicted	Actual
1	30.0	3.00	70	56.66	59.97
2	30.0	0.50	70	8.74	7.59
3	41.9	1.51	100	33.62	33.05
4	18.1	4.49	40	97.11	98.85
5	30.0	3.00	70	56.66	59.79
6	30.0	3.00	70	56.66	56.65
7	30.0	3.00	20	47.37	45.87
8	30.0	5.50	70	95.80	95.28
9	41.9	4.49	40	64.39	64.12
10	30.0	3.00	70	56.66	54.13
11	41.9	1.51	40	15.49	21.39
12	30.0	3.00	120	69.03	68.87
13	10.0	3.00	70	87.45	91.24
14	30.0	3.00	70	56.66	56.92
15	18.1	1.51	100	50.10	51.55
16	18.1	4.49	100	104.73	100.00
17	30.0	3.00	70	56.66	52.79
18	18.1	1.51	40	34.16	30.26
19	50.0	3.00	70	46.08	40.62
20	41.9	4.49	100	74.20	79.28

The second-order polynomial equation for IC degradation efficiency in terms of coded factors is given below as Eq. (5):

$$Y = 56.66 - 12.30 * A + 25.88 * B + 6.44 * C - 3.51 * A * B + 0.55 * A * C - 2.08 * B * C + 3.57 * A^2 - 1.55 * B^2 + 0.54 * C^2 \quad (5)$$

The predicted response, indicating the percentage of IC degradation, is denoted by the variable Y. The dye concentration, catalyst volume, and reaction time are represented by the variables A, B, and C, respectively. Catalyst volume (B) has the highest coefficient indicating that it has the greatest impact, as shown in Eq. (5). The positive coefficient indicates that high catalyst volume values favored IC degradation. Another factor that affected the response was the concentration of dye (A). A negative coefficient indicates that an increase in dye concentration will result in a decreased IC degradation. The coefficient of reaction time (C) has the minimum value indicating that it has least impact on the degradation of IC dye. The presence of a positive coefficient shows that higher reaction time values were beneficial for the degradation of IC [51]. Adequacy of the model was assessed using ANOVA. Table 5 displays the ANOVA results regarding the degradation of IC dye.

Table 5 ANOVA for the photocatalytic degradation of IC dye

Source	SS	df	MS	F-Value	p-Value	Remark
Model	12154.95	9	1350.55	69.57	< 0.0001	significant
A	2065.40	1	2065.40	106.40	< 0.0001	
B	9148.87	1	9148.87	471.31	< 0.0001	
C	566.29	1	566.29	29.17	0.0003	
AB	98.70	1	98.70	5.08	0.0478	
AC	2.40	1	2.40	0.12	0.7325	
BC	34.63	1	34.63	1.78	0.2113	
A^2	183.820	1	183.820	9.47	0.0117	
B^2	34.729	1	34.729	1.79	0.2107	
C^2	4.268	1	4.268	0.22	0.6492	
Residual	194.12	10	19.41			
Lack of Fit	151.87	5	30.37	3.59	0.0933	not significant
Pure Error	42.25	5	8.45			
Cor Total	12349.07	19				

SS: sum of squares; df: degrees of freedom; MS: mean square; F: frequency; p: probability; $R^2 = 0.9843$; Pred $R^2 = 0.8928$; Adj $R^2 = 0.9701$; C.V.=7.54; Adeq Precision=30.8105.

A p-value less than 0.05 indicates that the second-order polynomial model adequately describes the experimental data. The impact of model terms on the degradation of IC, as indicated by the p-values in Table 5, follows the order: B > A > C > A^2 > AB > B^2 > BC > C^2 > AC. The statistical significance of the model can be established by its high F-value (69.57) and a low p-value (<0.0001), which implies that model parameters including *A, B, C, AB, A²* are significant [52, 53]. The terms B^2, C^2, AC, and BC are not statistically significant as their p-values are more than 0.05, and hence they may be eliminated from Equation (5). Moreover, the importance of the model can be verified using the lack of fit test. The lack of fit is considered insignificant due to its p-value being higher than 0.05. The low coefficient of variation (C.V.) value of 7.54% confirms the model's accuracy. The signal-to-noise ratio of 30.8105 was considered adequate based on the results [53]. Furthermore, the fit of the model was validated by the coefficient of determination (R^2). The predicted R^2 value of 0.8929 (Table 5) for the model is consistent with the adjusted R^2 value of 0.9701, suggesting that the obtained model is statistically significant. The response (degradation efficiency) and the parameters have a good relationship (R^2 = 0.9843) according to Equation (5), as shown in Figure (4b). The figure displays a plot between the experimental and predicted values of IC degradation, which were generated from the RSM model. The percentage IC degradation values show a good fit [53].

3.2.2 Effect and interaction of factors on IC dye degradation

The interaction between catalyst volume and dye concentration (AB) is illustrated in Figure 5(a) in 3D surface plots. Dye degradation appears to increase with catalyst volume, whereas it decreases as dye concentration increases. Increased catalyst volume could be due to the large number of active sites present on nanoparticle surfaces, which allows more solar light to pass the aqueous solution. AgNPs absorb visible and ultraviolet radiation from solar light, which generates an abundance of reactive radicals [54]. The reactive radicals degrade and attack the IC dye molecules. As a result, this leads to higher degradation efficiency [52, 54]. The impact of dye concentration and reaction time on IC degradation is illustrated in Figure 5(b). Degradation of IC increases slightly with reaction time. An increase in dye concentration leads to decreased IC degradation. This may be a result of insufficient active sites, which are necessary for the high concentration of dye. When the concentration of dye increases, more dye molecules adhere to the catalyst surfaces. Generation of hydroxyl radicals is reduced due to the occupation of active sites by dye molecules [52]. This leads to an increased demand for reactive species such as $HO^{\cdot}$ and O_2^{-}, which are necessary for breaking down the dye. The catalyst's surface maintains a constant generation of $HO^{\cdot}$ and O_2^{-} when the catalyst dose and reaction time remain constant. Consequently, the number of active radicals available is insufficient to break down the dye when it is present in higher concentrations. Furthermore, reduced hyroxyl radical production at the catalyst surface is a result of photon absorption by the IC dye [52]. Therefore, the effectiveness of degradation decreases as the concentration of dye increases. The effects of reaction time and catalyst volume on IC dye degradation are displayed in Figure 5(c). Increased reaction time results in slightly increased degradation efficiency. This could be explained by the fact that the AgNPs photocatalyst surfaces are exposed to more solar light during longer irradiation times, which produces more hydroxyl radicals and increases the degradation of IC dye [52]. Furthermore, when the reaction time increases, the removal efficiency also increases. Free radical formation and hydroxyl radical creation may occur over extended periods of contact. The process may continue until a certain point, after which the growth rate becomes smoother as free radicals and pollutant degradation approach equilibrium [55, 56]. Previous research has revealed that increased contact duration results in enhanced removal efficiency [54, 57].

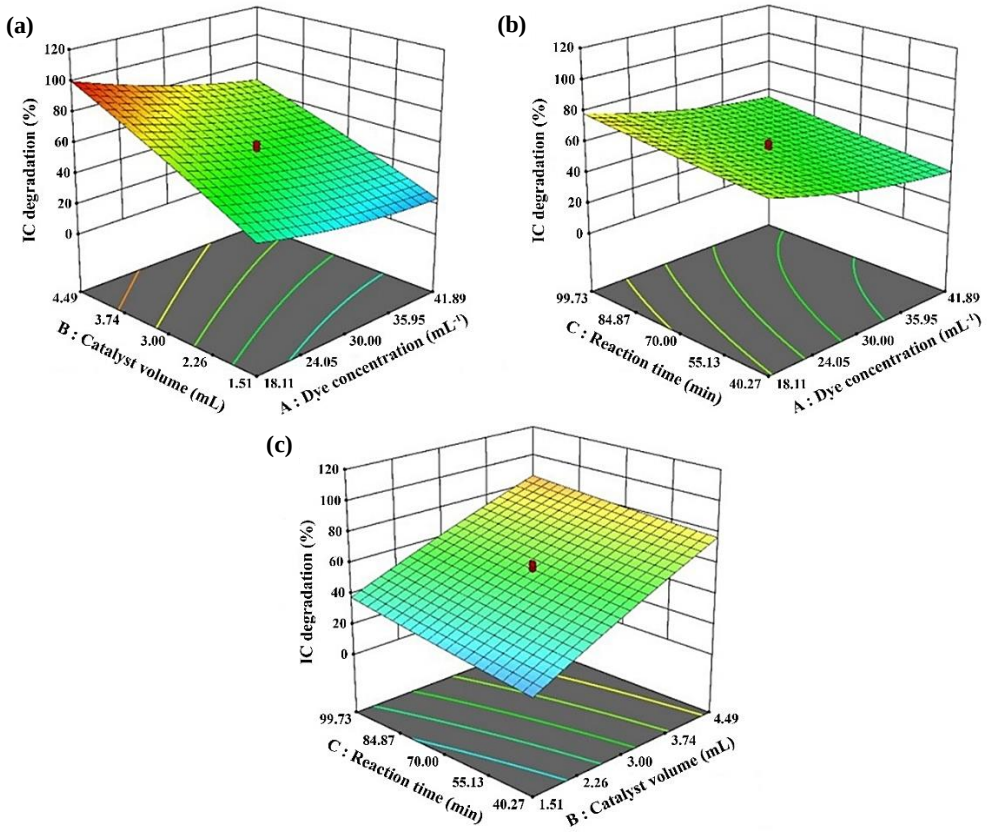

Figure 5 3D plots of interaction between dye concentration and catalyst volume (a), 3D plots of interaction between dye concentration and reaction time (b), and 3D plots of interaction between catalyst volume and reaction time (c) for the photocatalytic degradation of IC dye

To confirm the suitability of the RSM model, the model equation was employed to determine the optimal values for IC dye concentration, catalyst volume, and reaction time, resulting in the maximum degradation of IC dye. The optimal operating conditions in this investigation were an IC dye concentration of 19.7 mgL^{-1}, a catalyst volume of 4.47 mL, and a reaction time of 97 min. At these optimal conditions, the percentage IC dye degradation values for predicted and experimental data were 100.90% and 97.52%, respectively. The measured IC dye degradation values exhibited a deviation of less than 5% from the expected values. Thus, RSM successfully confirmed the optimum operating point, suggesting that it can be a useful tool for optimizing photocatalytic processes. Additionally, the developed model can be applied to any set of parameters within a specified range to minimize parameters or maximize the degradation efficacy of IC dye [53]. This result showed that the IC dye molecules completely degraded when reacted with the synthesized AgNP catalyst after 97 min under solar irradiation. Green synthesized AgNPs from different plant extracts exhibit promising performance for photocatalytic degradation of dye under solar irradiation. This work shows high efficiency in the rapid degradation of dyes when compared to other photocatalysts from different plant extracts as shown in Table 6.

Table 6 Comparison of green synthesized AgNPs from different plant extracts when used as catalysts for photocatalytic degradation

Plants	Dye and concentration	Light source and time	%Degradation	Ref.
Valeriana jatamansi	RhB 10 mgL^{-1}	Solar light 75 min	95%	[13]
Eucalyptus globulus	IC 10 mgL^{-1}	Solar light, 120 min	98%	[58]
Eucalyptus globulus	IC 10 mgL^{-1}	Solar light 75 min	100%	[59]
Capparis moonii	RB 10 mgL^{-1}	Solar light 60 min	100%	[60]
Moringa oleifera	MB 20 mgL^{-1}	Solar light 60 min	93%	[61]
Leucaena leucocephala	IC 19.7 mgL^{-1}	Solar light 97 min	97.52%	This work

3.2.3 Kinetics study

IC dye degradation was analyzed using kinetics models, specifically the pseudo-first order and pseudo-second order models (Figure 6). The pseudo-first order model showed a higher coefficient of determination (R^2 = 0.9610) compared to the pseudo-second order model (R^2 = 0.8029). Physisorption is a weak adsorption process that involves van der Waals interactions between the absorbent and adsorbate, and it is described by the pseudo-first order model. When the solute concentration is low or equilibrium is reached, this process can occur [62]. A rate constant of 0.1631 min^{-1} was obtained using the pseudo-first order model.

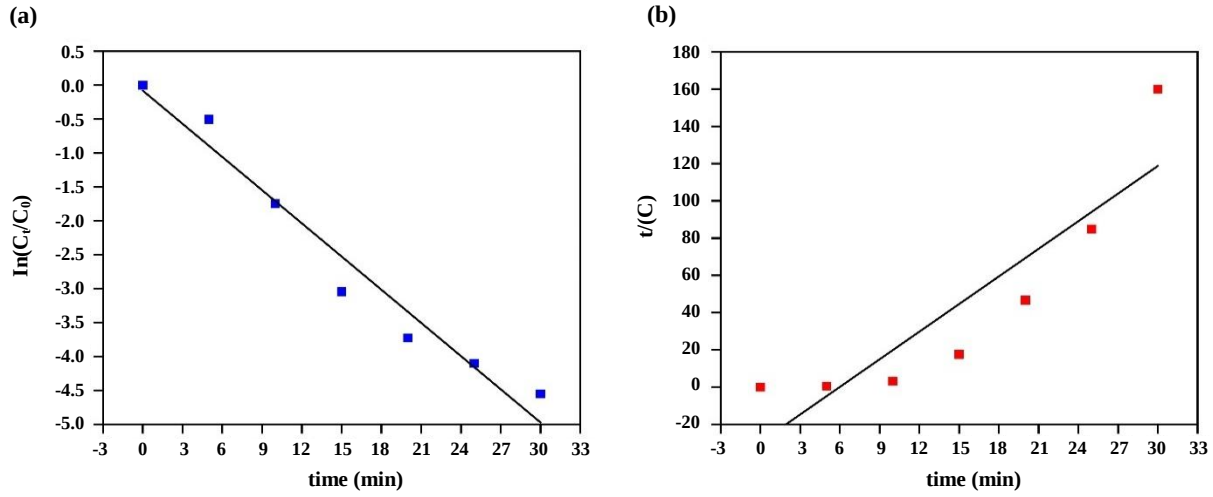

Figure 6 The plots of pseudo-first order (a), and pseudo-second order (b) models

3.2.4 A proposed mechanism for the photocatalytic breakdown of IC dye

A possible mechanism for the photocatalytic degradation of IC dye is shown in Figure 7. Photoexcited holes and electrons are formed in the valence band (VB) and the conduction band (CB) of silver nanoparticles. This phenomenon occurs after irradiation of the AgNP nanocatalysts [8]. The reaction primarily occurs at nanoparticle surfaces, where electrons in the valence band (*VB*) are excited and transition to the conduction band (*CB*) upon exposure to solar irradiation. A positive hole (h^+) is produced in the *VB*, while a conduction electron (e^-) is generated in the *CB*. The presence of h^+ and e^- involves production of reactive radicals to degrade IC dye in the mixture solution. The h^+ interacts with water molecules, leading to the generation of hydroxyl radicals ($HO\cdot$) and hydrogen ions (H^+). Additionally, the e^- of AgNPs converts dissolved oxygen (O_2) into superoxide radical anions (O_2^-). Furthermore, the O_2^- reacts with water molecules, resulting in the production of $HO\cdot$ and hydroperoxyl (HO_2^-) radicals as final products. Photocatalytic degradation of IC dye is significantly influenced by three photogenerated radicals, $HO\cdot$, O_2^-, and HO_2^- [63, 64]. The proposed mechanism for the degradation process of the IC dye is described in Equations (6) to (10).

$$Ag^0 + hv \rightarrow e^-(CB) + h^+(VB) \quad (6)$$

$$h^+(VB) + H_2O \rightarrow H^+ + HO^\cdot \quad (7)$$

$$e^-(CB) + O_2 \rightarrow O_2^{\cdot-} \quad (8)$$

$$O_2^{\cdot-} + H_2O \rightarrow HO^\cdot + HO_2^- \quad (9)$$

$$HO^\cdot + O_2^{\cdot-} + HO_2^- + IC \rightarrow Degradation\ products \quad (10)$$

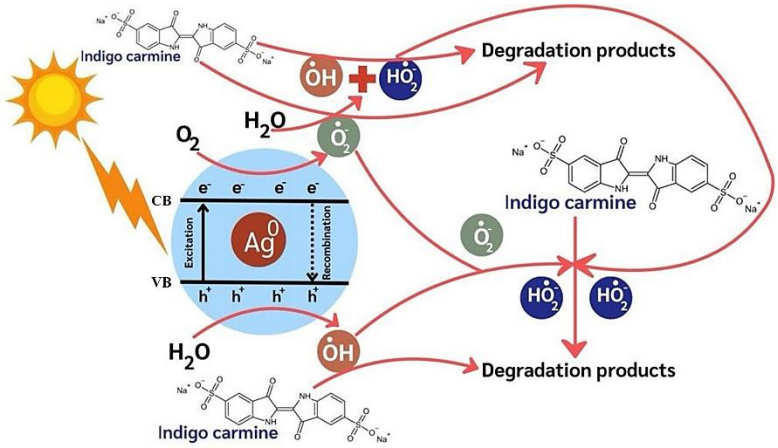

Figure 7 Proposed mechanism of photocatalytic degradation of IC dye (modified from Fouladi-Fard et al. [8], and Shaikh et al. [63])

4. Conclusions

AgNPs were successfully synthesized using *Leucaena leucocephala* leaf extract due to its phenolic compounds, which act as reducing and capping agents. Moreover, the results demonstrate that spherical-shaped crystalline nanoparticles with an average diameter of 7.29±0.05 nm, contain the silver element as supported by the above experimental results. The efficiency of green synthesized AgNPs was assessed for the photocatalytic degradation of IC dye under solar irradiation using RSM based on a CCD design. The optimal conditions for the process were a dye concentration of 19.7 mgL^{-1}, catalyst volume of 4.47 mL, and reaction time of 97 min, achieving a photocatalytic efficiency of 97.52%. Moreover, the pseudo-first order model was appropriate for fitting photocatalytic degradation of IC dye, indicating that the rate of reaction depends on initial substrate concentration. It can be concluded that the leaf extract of *Leucaena leucocephala* is reliable in producing AgNPs for removing IC dye from textile industry effluents. The current study will aid in the manufacture of value-added products from *Leucaena leucocephala*, supporting the environment and nanotechnology.

5. Acknowledgements

Chaison P, Wittayanarakul K, and Sriuttha M thank Research and Graduate Studies (RP64-4-002), Khon Kaen University for their financial support.

6. References

[1] Mazhar S, Qazi UY, Nadeem N, Zahid M, Jalili A, Khan F, et al. Photocatalytic degradation of methylene blue using polyaniline-based silver-doped zinc sulfide (PANI-Ag/ZnS) composites. Environ Sci Pollut Res. 2022;29(6):9203-17.
[2] Brudzyńska P, Sionkowska A, Grisel M. Plant-derived colorants for food, cosmetic and textile industries: a review. Materials. 2021;14(13):3484.
[3] Nohynek GJ, Antignac E, Re T, Toutain H. Safety assessment of personal care products/cosmetics and their ingredients. Toxicol Appl Pharmacol. 2010;243(2):239-59.
[4] Nekouei F, Noorizadeh H, Nekouei S, Asif M, Tyagi I, Agarwal S, et al. Removal of malachite green from aqueous solutions by cuprous iodide-cupric oxide nano-composite loaded on activated carbon as a new sorbent for solid phase extraction: Isotherm, kinetics and thermodynamic studies. J Mol Liq. 2016;213:360-8.
[5] Ahmed MA, brick AA, Mohamed AA. An efficient adsorption of indigo carmine dye from aqueous solution on mesoporous Mg/Fe layered double hydroxide nanoparticles prepared by controlled sol-gel route. Chemosphere. 2017;174:280-8.
[6] Adel M, Ahmed MA, Mohamed AA. Effective removal of indigo carmine dye from wastewaters by adsorption onto mesoporous magnesium ferrite nanoparticles. Environ Nanotechnol Monit Manage. 2021;16:100550.
[7] Salem ANM, Ahmed MA, El-Shahat MF. Selective adsorption of amaranth dye on Fe_3O_4/MgO nanoparticles. J Mol Liq. 2016;219:780-8.
[8] Fouladi-Fard R, Aali R, Mohammadi-Aghdam S, Mortazavi-derazkola S. The surface modification of spherical ZnO with Ag nanoparticles: A novel agent, biogenic synthesis, catalytic and antibacterial activities. Arab J Chem. 2022;15(3):103658.
[9] Hashemi Z, Shirzadi-Ahodashti M, Mortazavi-Derazkola S, Ebrahimzadeh MA. Sustainable biosynthesis of metallic silver nanoparticles using barberry phenolic extract: optimization and evaluation of photocatalytic, in vitro cytotoxicity, and antibacterial activities against multidrug-resistant bacteria. Inorg Chem Commun. 2022;139:109320.

[10] Khan KA, Shah A, Nisar J, Haleem A, Shah I. Photocatalytic degradation of food and juices dyes via photocatalytic nanomaterials synthesized through green synthetic route: a systematic review. Molecules. 2023;28(12):4600.
[11] Kareem MA, Bello IT, Shittu HA, Sivaprakash P, Adedokun O, Arumugam S. Synthesis, characterization, and photocatalytic application of silver doped zinc oxide nanoparticles. Clean Mater. 2022;3:100041.
[12] Princy SSJ, Hentry C, Alodaini HA, Hatamleh AA, Arokiyaraj S, Bindu MR. *Hibiscus cannabinus* seeds assisted spherical silver nanoparticles and its antibacterial and photocatalytic applications. Chem Phys Impact. 2023;6:100192.
[13] Prem P, Naveenkumar S, Kamaraj C, Ragavendran C, Priyadharsan A, Manimaran K, et al. *Valeriana jatamansi* root extract a potent source for biosynthesis of silver nanoparticles and their biomedical applications, and photocatalytic decomposition. Green Chem Lett Rev. 2024;17(1):2305142.
[14] Venkatesan S, Suresh S, Arumugam J, Ramu P, Pugazhenthiran N, Jothilakshmi R, et al. Sunlight assisted degradation of methylene blue dye by zinc oxide nanoparticles green synthesized using *Vitex negundo* plant leaf extract. Results Chem. 2024;7:101315.
[15] Hadi AA, Ng JY, Shamsuddin M, Matmin J, Malek NANN. Green synthesis of silver nanoparticles using *Diplazium esculentum* extract: catalytic reduction of methylene blue and antibacterial activities. Chem Pap. 2022;76:65-77.
[16] Mustapha T, Misni N, Ithnin NR, Daskum AM, Unyah NZ. A review on plants and microorganisms mediated synthesis of silver nanoparticles, role of plants metabolites and applications. Int J Environ Res Public Health. 2022;19(2):674.
[17] Basalius H, Mani A, Michael A, Mary SM, Lenin M, Chelliah P, et al. Green synthesis of nano-silver using *Syzygium samarangense* flower extract for multifaceted applications in biomedical and photocatalytic degradation of methylene blue. Appl Nanosci. 2023;13(3):3735-3747.
[18] Zabihi MM, Eghbaliferiz S, Khorashadizadeh M, Mortazavi-Derazkola S, Yousefi M. Green synthesis of non-toxic silver nanoparticles using *Salvia tebesana* Bunge extract: Optimization, cytotoxicity, and antibacterial activities. Results Chem. 2024;7:101510.
[19] Zare-Bidaki M, Aramjoo H, Mizwari ZM, Mohammadparast-Tabas P, Javanshir R, Mortazavi-Derazkola S. Cytotoxicity, antifungal, antioxidant, antibacterial and photodegradation potential of silver nanoparticles mediated via *Medicago sativa* extract. Arab J Chem. 2022;15(6):103842.
[20] Younas M, Rasool MH, Khurshid M, Khan A, Nawaz MZ, Ahmad I, et al. *Moringa oleifera* leaf extract mediated green synthesis of silver nanoparticles and their antibacterial effect against selected gram-negative strains. Biochem Syst Ecol. 2023;107:104605.
[21] Khatun M, Khatun Z, Karim MR, Habib MR, Rahman MH, Aziz MA. Green synthesis of silver nanoparticles using extracts of *Mikania cordata* leaves and evaluation of their antioxidant, antimicrobial and cytotoxic properties. Food Chemi Adv. 2023;3:100386.
[22] Sikdar S, Sikdar M. Green synthesis, optimization and analyzing of silver nanoparticles encapsulated with *Syzygium aromaticum* extract: Evaluating antibacterial and photocatalytic properties. Bioresour Technol Rep. 2023;24:101669.
[23] Raju S, Ashok D, Boddu AR. *Leucaena Leucocephala* mediated green synthesis of silver nanoparticles and their antibacterial, dye degradation and antioxidant properties. Int J Nanosci Nanotechnol. 2022;18(1):65-78.
[24] Kato-Noguchi H, Kurniadie D. Allelopathy and Allelochemicals of *Leucaena leucocephala* as an Invasive Plant Species. Plants (Basel). 2022;11(13):1672.
[25] Elbanoby NE, El-Settawy AAA, Mohamed AA, Salem MZM. Phytochemicals derived from *Leucaena leucocephala* (Lam.) de Wit (Fabaceae) biomass and their antimicrobial and antioxidant activities: HPLC analysis of extracts. Biomass Convers Biorefin. 2024;14:14593-609.
[26] Sharma K, Guleria S, Salaria KH, Majeed A, Sharma N, Pawar KD, et al. Photocatalytic and biological properties of silver nanoparticles synthesized using *Callistemon lanceolatus* leaf extract. Ind Crops Prod. 2023;202:116951.
[27] Sudarjanto G, Keller-Lehmann B, Keller J. Optimization of integrated chemical-biological degradation of a reactive azo dye using response surface methodology. J Hazard Mater. 2006;138(1):160-8.
[28] Njagi EC, Huang H, Stafford L, Genuino H, Galindo HM, Collins JB, et al. Biosynthesis of iron and silver nanoparticles at room temperature using aqueous sorghum bran extracts. Langmuir. 2011;27(1):264-71.
[29] Chen L, Huo Y, Han YX, Li JF, Ali H, Batjikh I, et al. Biosynthesis of gold and silver nanoparticles from *Scutellaria baicalensis* roots and in vitro applications. Appl Phys A. 2020;126(6):424.
[30] Murshed MK, Dursun AY, Dursun G. Application of response surface methodology on photocatalytic degradation of Astrazon Orange G dye by ZnO photocatalyst: internal mass transfer effects. Chem Eng Res Des. 2022;188:27-38.
[31] Shah MZ, Guan ZH, Din AU, Ali A, Rehman AU, Jan K, et al. Synthesis of silver nanoparticles using *Plantago lanceolata* extract and assessing their antibacterial and antioxidant activities. Sci Rep. 2021;11:20754.
[32] Favier L, Simion AI, Hlihor RM, Fekete-Kertész I, Molnár M, Harja M, et al. Intensification of the photodegradation efficiency of an emergent water pollutant through process conditions optimization by means of response surface methodology. J Environ Manage. 2023;328:116928.
[33] Saratale RG, Cho SK, Saratale GD, Kadam AA, Ghodake GS, Magotra VK, et al. Lignin-mediated silver nanoparticle synthesis for photocatalytic degradation of reactive yellow 4G and in vitro assessment of antioxidant, antidiabetic, and antibacterial activities. Polymers. 2022;14(3):648.
[34] Mehwish HM, Rajoka MSR, Xiong Y, Cai H, Aadil RM, Mahmood Q, et al. Green synthesis of a silver nanoparticle using *Moringa oleifera* seed and its applications for antimicrobial and sun-light mediated photocatalytic water detoxification. J Environ Chem Eng. 2021;9(4):105290.
[35] Awad MA, Hendi AA, Ortashi KM, Alzahrani B, Soliman D, Alanazi A, et al. Biogenic synthesis of silver nanoparticles using *Trigonella foenum-graecum* seed extract: characterization, photocatalytic and antibacterial activities. Sens Actuators A: Phys. 2021;323(5):112670.
[36] Chandrika KC, Prabhu TN, Kiran RRS, Krishna RH. Applications of artificial neural network and box-behnken design for modelling malachite green dye degradation from textile effluents using TiO_2 photocatalyst. Environ Eng Res. 2022;27(1):200553.
[37] Yusoff SFM, Firdaus F, Zahidi NAA, Halim NHA. Optimization, kinetics isotherm, and reusability studies of methylene blue dye adsorption using acrylic acid grafted rubber hydrogel. Sains Malays. 2022;51(10):3307-20.
[38] Agnihotri S, Sillu D, Sharma G, Arya RK. Photocatalytic and antibacterial potential of silver nanoparticles derived from pineapple waste: process optimization and modeling kinetics for dye removal. Appl Nanosci. 2018;8:2077-92.

[39] Nazim M, Khan AAP, Asiri AM, Kim JH. Exploring rapid photocatalytic degradation of organic pollutants with porous CuO nanosheets: synthesis, dye removal, and kinetic studies at room temperature. ACS Omega. 2021;6(4):2601-12.
[40] Khane Y, Benouis K, Albukhaty S, Sulaiman GM, Abomughaid MM, Ali AA, et al. Green synthesis of silver nanoparticles using aqueous *Citrus limon* zest extract: characterization and evaluation of their antioxidant and antimicrobial properties. Nanomaterials (Basel). 2022;12(12):2013.
[41] Saied E, Hashem AH, Ali OM, Selim S, Almuhayawi MS, Elbahnasawy MA. Photocatalytic and antimicrobial activities of biosynthesized silver nanoparticles using *Cytobacillus firmus*. Life. 2022;12(9):1331.
[42] Ali F, Younas U, Nazir A, Hassan F, Iqbal M, Hamza B, et al. Biosynthesis and characterization of silver nanoparticles using strawberry seed extract and evaluation of their antibacterial and antioxidant activities. J Saudi Chem Soc. 2022;26(6):101558.
[43] Kumar R, Sharma P, Bamal A, Negi S, Chaudhary S. A safe, efficient and environment friendly biosynthesis of silver nanoparticles using *Leucaena leucocephala* seed extract and its antioxidant, antimicrobial, antifungal activities and potential in sensing. Green Process Synth. 2017;6(5):449-59.
[44] Ghotekar S, Savale A, Pansambal S. Phytofabrication of fluorescent silver nanoparticles from *Leucaena leucocephala* L. leaves and their biological activities. J Water Environ Nanotechnol. 2018;3(2):95-105.
[45] Meng Y. A sustainable approach to fabricating Ag nanoparticles/PVA hybrid nanofiber and its catalytic activity. Nanomaterials (Basel). 2015;5(2):1124-35.
[46] Nayab D, Akhtar S. Green synthesized silver nanoparticles from eucalyptus leaves can enhance shelf life of banana without penetrating in pulp. PLOS ONE. 2023;18(3):e0281675.
[47] Ali MH, Azad MAK, Khan KA, Rahman MO, Chakma U, Kumer A. Analysis of crystallographic structures and properties of silver nanoparticles synthesized using PKL extract and nanoscale characterization techniques. ACS Omega. 2023;8(31):28133-42.
[48] Majoumouo MS, Tincho MB, Yimta YD, Adekiya TA, Aruleba RT, Ayawei N, et al. Biosynthesis of silver nanoparticles using *Bersama engleriana* fruits extracts and their potential inhibitory effect on resistant bacteria. Crystals. 2022;12(7):1010.
[49] Naghdali Z, Sahebi S, Ghanbari R, Mousazadeh M, Jamali HA. Chromium removal and water recycling from electroplating wastewater through direct osmosis: modeling and optimization by response surface methodology. Environ Health Eng Manag. 2019;6(2):113-20.
[50] Hong GB, Wang YK. Synthesis of low-cost adsorbent from rice bran for the removal of reactive dye based on the response surface methodology. Appl Surf Sci. 2017;423:800-9.
[51] Dinari A, Mamoudi J. Response surface methodology analysis of the photodegradation of methyl orange dye using synthesized TiO_2/Bentonite/ZnO composites. Adv Environ Technol. 2022;8(1):31-46.
[52] Ekka B, Sahu MK, Patel RK, Dash P. Titania coated silica nanocomposite prepared via encapsulation method for the degradation of safranin-O dye from aqueous solution: optimization using statistical design. Water Resour Ind. 2019;22:100071.
[53] Rana AG, Minceva M. Analysis of photocatalytic degradation of phenol with exfoliated graphitic carbon nitride and light-emitting diodes using response surface methodology. Catalyst. 2021;11(8):898.
[54] Sahragard S, Naghizadeh A, Mortazavi-Derazkola S, Derakhshani E. Detoxifcation of Trimethoprim antibiotic using $NiFe_2O_4$@MoO_3 magnetic nanocomposites phyto-synthesized with green route: experimental and RSM modeling. BioNanoScience. 2024;14:1119-31.
[55] Dehghan A, Zarei A, Jaafari J, Shams M, Khaneghah AM. Tetracycline removal from aqueous solutions using zeolitic imidazolate frameworks with different morphologies: a mathematical modeling. Chemosphere. 2019:217:250-60.
[56] Phuong NM, Chu NC, Thuan DV, Ha MN, Hanh NT, Viet HDT, et al. Novel removal of diazinon pesticide by adsorption and photocatalytic degradation of visible light-driven Fe-TiO_2/Bent-Fe photocatalyst. J Chem. 2019;2019(1):1-7.
[57] Hossienzadeh K, Maleki A, Daraei H, Safari M, Pawar R, Lee SM. Sonocatalytic and photocatalytic efficiency of transition metal-doped ZnO nanoparticles in the removal of organic dyes from aquatic environments. Korean J Chem Eng. 2019;36:1360-70.
[58] Rocha V, Ferreira-Santos P, Genisheva Z, Coelho E, Neves IC, Tavares T. Environmental remediation promoted by silver nanoparticles biosynthesized by eucalyptus leaves extract. J Water Process Eng. 2023;56:104431.
[59] Rocha V, Ferreira-Santos P, Aguiar C, Neves IC, Tavares T. Valorization of plant by-products in the biosynthesis of silver nanoparticles with antimicrobial and catalytic properties. Environ Sci Pollut Res. 2024;31(9):14191-207.
[60] Annigol LB, Sajjan VP, Gurubasavaraj PM, Ganachari SV, Patil D. Study on the effect of pH on the biosynthesis of silver nanoparticles using *Capparis moonii* fruit extract: their applications in anticancer activity, biocompatibility and photocatalytic degradation. Chem Pap. 2023;77(12):3327-45.
[61] Ghosh T, Chattopadhyay A, Pramanik S, Das S, Mukherjee S, Mandal AC, et al. Biosynthesis of highly stable silver nanoparticles for enhanced antibacterial effect and efficient photocatalytic for dye degradation. Braz J Phys. 2024;54:9.
[62] Mittal H, Kumar A, Khanuja M. In-situ oxidative polymerization of aniline on hydrothermally synthesized $MoSe_2$ for enhanced photocatalytic degradation of organic dyes. J Saudi Chem Soc. 2019;23(7):836-45.
[63] Shaikh WA, Chakraborty S, Islam RU. Photocatalytic degradation of rhodamine B under UV irradiation using *Shorea robusta* leaf extract-mediated bio-synthesized silver nanoparticles. Int J Environ Sci Technol. 2020;17:2059-72.
[64] Karthik R, Govindasamy M, Chen SM, Cheng YH, Muthukrishnan P, Padmavathy S, et al. Biosynthesis of silver nanoparticles by using *Camellia japonica* leaf extract for the electrocatalytic reduction of nitrobenzene and photocatalytic degradation of Eosin-Y. J Photochem Photobiol B: Biol. 2017;170:164-72.